Jinst

Published by IOP Publishing for Sissa Medialab

Received: *March 2, 2021*
Accepted: *March 21, 2021*
Published: *March 31, 2021*

ICFA Beam Dynamics Newsletter#81 —
Electron Lenses for Modern and Future Accelerators

Hollow electron lenses for beam collimation at the High-Luminosity Large Hadron Collider (HL-LHC)

S. Redaelli,[a,1,*] **R.B. Appleby,**[b] **R. Bruce,**[a] **O. Brüning,**[a] **A. Kolehmainen,**[a] **G. Ferlin,**[a] **A. Foussat,**[a] **M. Giovannozzi,**[a] **P. Hermes,**[a] **D. Mirarchi,**[a,c] **D. Perini,**[a] **A. Rossi**[a] **and G. Stancari**[c]

[a] *European Organization for Nuclear Research, Esplanade des Particules 1, 1211 Meyrin, Geneva, Switzerland*
[b] *Fermi National Accelerator Laboratory, P.O. Box 500, Batavia, Illinois 60510, U.S.A.*
[c] *The University of Manchester and the Cockcroft Institute, Oxford Road, Manchester, M13 9PL, U.K.*

E-mail: Stefano.Redaelli@cern.ch

Abstract: Electrons lenses produce a high-intensity electron beam and have a variety of applications to circular hadron accelerators. Electron beams of different transverse cross sections and distributions may be designed, depending on the desired application, and they are produced and steered along the orbit of the hadron beam, overlapping with it for typical distances of a few meters before being deflected away and disposed of. Hollow electron beams find applications to high-intensity beam collimation for machines like the CERN Large Hadron Collider (LHC). Such devices can be integrated in a collimation system to improve the halo-cleaning performance through an active control of the halo dynamics: the annular distribution of the electrons excites resonantly the beam tails surrounding the beam core, while the core itself remains unperturbed, as ideally it only "sees" the field-free "hole" in the electron distribution. Hollow electron lenses are part of the upgrade baseline of the High-Luminosity project of the LHC (HL-LHC) and will be installed in the machine during a long shutdown in 2025–2027 to mitigate effects from beam losses so to improve the collimation system performance. This paper describes the hollow electron lens project within the HL-LHC collimation upgrade.

Keywords: Accelerator Applications; Accelerator modelling and simulations (multi-particle dynamics; single-particle dynamics); Accelerator Subsystems and Technologies; Beam dynamics

[1] Work supported by the HL-LHC project.
[*] Corresponding author.

https://doi.org/10.1088/1748-0221/16/03/P03042

2021 JINST 16 P03042

Contents

1 Introduction

The Large Hadron Collider (LHC) [1] at the European Organization for Nuclear Research (CERN) is designed to collide two 7 TeV proton beams, each carrying the unprecedented stored-beam energy of 362 MJ. The LHC will start its third Run in 2022 after the very successful Run 1 (2010-2013) with beam energies up to 4 TeV and Run 2 (2015–2018) with beam energies up to 6.5 TeV. Starting in 2025, it is planned to upgrade the LHC according to the High-Luminosity (HL-LHC) upgrade project [2], aiming at nearly doubling the beam current, while reducing by more than 30% the beam emittance compared to the LHC design value. This goal will be achieved thanks to the implemented LHC Injectors Upgrade project [3]. The ambitious goal of the HL-LHC project is to accumulate an integrated luminosity of approximately 3000 fb^{-1} until about 2040, i.e. to reach a total of about ten times more than what is expected to be accumulated by the end of Run 3 in 2024. Beam losses are also a concern for the operation at the LHC with heavy-ion beams. Although the target total stored energy is about 20 MJ, the beam collimation process is less efficient than for proton beams, so halo losses are also an important concern [4].

2021 JINST 16 P03042

The halo collimation of proton and ion beams in a superconducting accelerator like the LHC poses obvious concerns, and a sophisticated multi-stage collimation system has therefore been designed, installed, and successfully operated [5–11]. Even if the performance of the LHC collimation system so far was very good, as stored energies in excess of 300 MJ were routinely handled without quenches triggered by beam losses on the collimation system [12–14], uncertainties apply to the extrapolations to conditions at the HL-LHC, with doubled bunch current, smaller emittances, and higher beam energies. Various means to improve the LHC collimation performance are therefore under investigation [15]. Some important upgrades already took place in the LHC Long Shutdown 2, which covers the period 2019–2021, with a first phase of the planned low-impedance upgrade of the betatron collimators and with the improvement of the dispersion-suppressor cleaning [15].

A specific threat to an efficient operation of the HL-LHC was identified in sudden losses generated by fast transients, e.g. orbit jitters, in presence of highly-populated beam halos, generating fast losses that could result in magnet quenches or beam dumps. Although such effects were under good control in Run 2, a quantitative scaling of tail populations and in general of loss mechanisms to the challenging HL-LHC beam conditions is neither easy nor evident. If one simply assumes that the halo populations scale linearly with the total beam current, one can estimate that up to 36 MJ might be stored in the beam tail, i.e. above around 3 RMS beam sizes and very close to the aperture of the primary collimators [16, 17]. Note that this is more than 10 times larger than the total beam energy stored in the Tevatron beams [18, 19]. The HL-LHC project management recognized the need to put in place mitigation strategies to make the operation less sensitive to transient beam losses, following a review on the needs for active halo control at the LHC [20].

Hollow electron beams can boost the performance of a collimation system through an active control of halo particles' diffusion speed and the tail population. By creating an annular area around the beam core nearly free of halo particles, loss spikes are greatly suppressed. The hollow electron beams can be generated by a Hollow Electron Lens (HEL) that produces a low-energy electron beam with a cylindrical symmetry using a hollow cathode. The electron beam is deflected to run co-axially to the circulating hadron beam, over a few metres, such that it acts on the halo particles at transverse amplitudes below that of the primary collimators without perturbing the beam core, which propagates in the field-free region inside the hollow electron beam. The current multi-stage collimation system must remain in place to safely dispose of the halo particles that are resonantly driven unstable by the electron beam at smooth and controllable loss rates. In this scheme, the collimation system maintains its role to protect the ring from the standard loss mechanisms — other fast beam losses are affected little by the HEL that provides small kicks at every turn — but is not exposed to fast losses from transverse displacements of the halo, e.g. from beam-orbit jitters.

In this paper, the current design of the HEL for the HL-LHC is reported. After a description of the integration of a HEL-based collimation scheme in section 2, motivation and requirements for the HEL are presented in section 3. In section 4, the detailed design of the different HEL sub-systems is presented with the target performance reach. In section 5, the expected performance of the HEL at the HL-LHC is reviewed. Finally, some conclusions are drawn in section 6.

2021 JINST 16 P03042

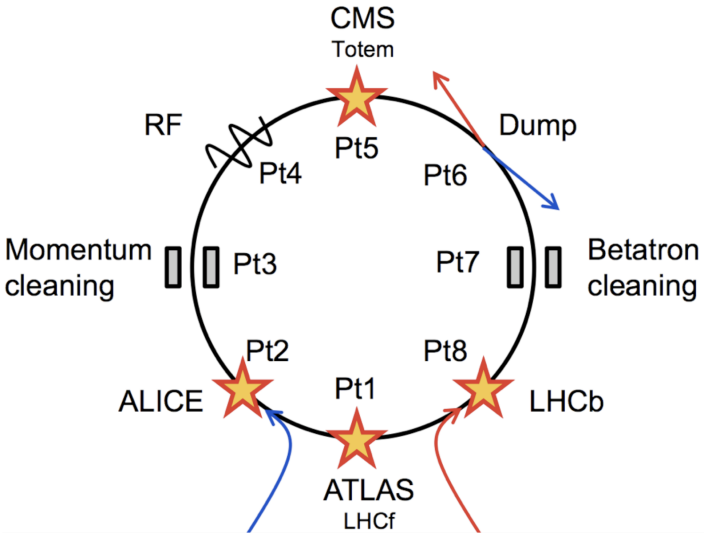

Figure 1. Schematic representation of the LHC ring. Beams are brought in collision in 4 straight sections in Pt1, Pt2, Pt5, and Pt8. The other straight sections house the collimation systems (Pt3, Pt7), the radio-frequency (RF) system and some instrumentation devices (Pt4), and the dump systems for both beams (Pt6). The counter-rotating Beam 1 (blue) and Beam 2 (red) are injected in Pt2 and Pt8, respectively. Pt4 will also house the HL-LHC hollow electron lenses.

2 HEL collimation scheme and integration in the HL-LHC collimation system

The layout of the LHC ring is shown in figure 1. The LHC is installed in a 27 km-long underground tunnel and it has an eight-fold symmetry with 8, 3.3 km-long arcs and 8 straight sections. The 4 main LHC experiments are housed in Pt1 (ATLAS), Pt2 (ALICE), Pt5 (CMS), and Pt8 (LHCb). Two straight sections with normal-conducting magnets are dedicated to beam collimation: Pt3 for momentum cleaning and Pt7 for betatron cleaning. Pt6 houses the beam dumping system. Finally, Pt4 is a straight section that houses the Radio-Frequency (RF) system and some instrumentation devices. The two counter-rotating LHC beams are injected in Pt2 (Beam 1, clockwise) and Pt8 (Beam 2, counter-clockwise). This layout will be preserved for the HL-LHC, with major upgrades taking place in Pt1 and Pt5 in order to enable improved luminosity performance for the two general-purpose experiments, ATLAS and CMS. Other important upgrades take also place in different parts of the ring, as described in detail in [2].

HELs provide a mechanism to control the diffusion speed of halo particles and therefore control how particles are driven towards the jaws of the collimators. The disposal of beam halos remains the responsibility of the existing collimation system. HELs are integrated in the transverse hierarchy of the betatron collimation system as illustrated in figure 2: they act on particles with transverse amplitudes just below those of the primary collimators (dark-gray box in the scheme). After the interaction with the primary collimators, the halo particles are disposed of through the standard multi-stage cleaning mechanisms [1]. We will see that the kick experienced by a halo particle at each passage through the HEL is of the order of a fraction of a microradian. This induces a moderate change in the halo particle's motion so that single-turn effects can be considered negligible. Therefore, HELs do not need to be located close to the collimation system and might be

2021 JINST 16 P03042

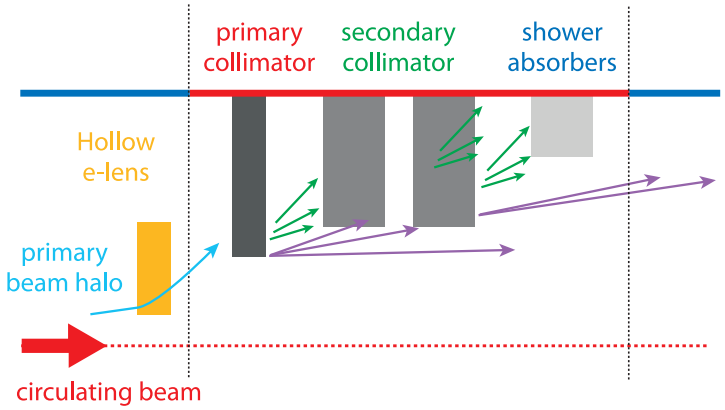

Figure 2. Scheme illustrating the conceptual integration of a HEL in the current collimation system hierarchy. The transverse amplitude range covered by the HEL (yellow) spans amplitudes between the tails of the circulating beam and those of the primary collimators (dark-grey) of the multi-stage collimation system. Their effect is to enhance the diffusion of halo particles that are sent in a controlled way on the betatron collimation system.

installed at any location around the ring. They do not produce local losses, and they are designed to have a negligible effect on fast losses. Suitable locations were found in Pt4 close to the main RF system. As discussed later, ensuring the electron beam stability requires intense solenoidal magnetic fields that will be achieved with superconducting magnets. The LHC Pt4 features already a cryogenics system and also has other advantages like the increased inter-beam distance, required by the RF system [1], that leaves more space for the integration of the lenses.

More details on the planned integration in Pt4 are discussed in section 4.6. Table 1 reports the main optical functions at the corresponding locations for both beams. An effort was made in matching the nominal optics to have round proton beams at the HEL location and to increase the β-functions while keeping a small dispersion. The layouts are symmetric for Beam 1 and Beam 2, and optimum conditions were achieved in the latest version of the HL-LHC optics, i.e. V1.5 [21]. The β-functions for both beams and planes in the Pt4 region are shown in figure 3, together with some layout elements in this region. Blue boxes indicate the "dogleg" dipoles that are used to increase the inter-beam distance in the straight region over a length of ≈ 100 m around Pt4 ($s = 9997.1$ m), as required for the LHC RF system [1].

3 HEL specifications for enhanced beam collimation

3.1 Motivations and required performance

The presence of highly populated beam tails risks making the operation very sensitive to small orbit jitters, naturally observed in the beam dynamics or triggered by different sources like earth quakes and power converter ripple [22]. Damage might also be caused in case of fast failure scenarios as potentially expected at the HL-LHC. Particular concerns arise for the operation of crab-cavities [23] that will also be installed starting in 2025 and will be used in the HL-LHC. These new devices have the potential to excite failures with the rise time of a few LHC turns [24], as well as from the risk of dumping asynchronously the two HL-LHC beams, which triggers a transverse kick on the beam

2021 JINST 16 P03042

Table 1. Main parameters at the locations of the HELs for Beam 1 and Beam 2. In the nominal optics, the relevant parameters are matched to the same values for the two beams, and for the horizontal and vertical planes.

Parameter	Value/range
Proton kinetic energy, E_{beam} [TeV]	7
Proton emittance (rms, normalized), ϵ [µm]	2.5
β-function at electron lens, $\beta_{x,y}$ [m]	280
Dispersion at electron lens, $D_{x,y}$ [m]	0.0
Proton beam size at electron lens, σ [µm]	306
Typical beam divergence (rms), σ' [µrad]	1.3–1.5
Diameter of the (warm) beam aperture, [mm]	60
Beam 1 longitudinal position from IP1, [m]	9957.0
Beam 2 longitudinal position from IP1, [m]	10037.2

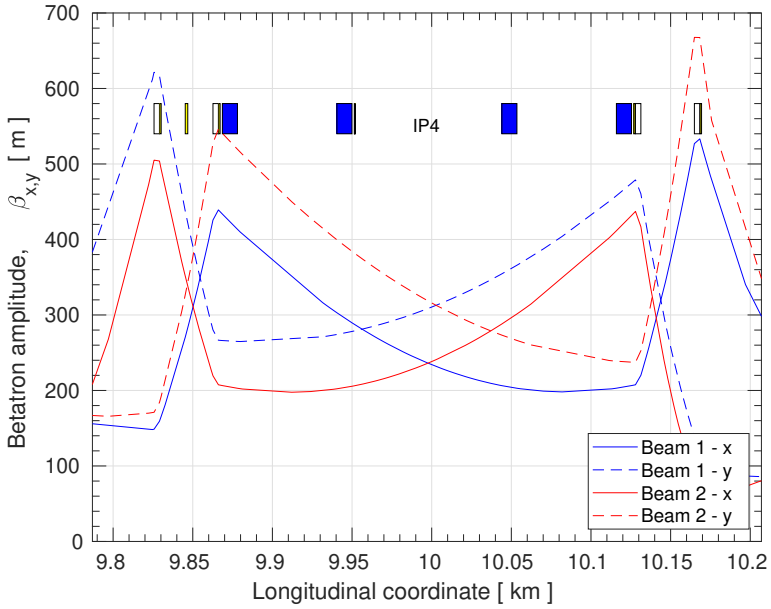

Figure 3. Evolution of the β-functions for both beams and planes in the Pt4 region [21]. Key layout elements are shown by the coloured boxed: dipole (blue) and quadrupoles (white) in the line. For both beams, the HELs are placed at the locations with round optics (see table 1).

that circulates for longer times (see [25] for an overview of various possible effects for HL-LHC). There is a solid experimental basis from measurements at the LHC that indicates consistently the presence of large tail populations [16, 17]: reducing the steady-state population of tails is important to mitigate known and unknown loss effects and might even become mandatory if some fast failure scenarios cannot be excluded.

In the end of Run 1 (2010-2013), the LHC operation at 4 TeV was severely affected by issues related to beam losses. The configuration of the collimation system was based on primary collimators at gap values close to ±1 mm, which intentionally equalled the nominal settings at 7 TeV. The situation significantly improved in the Run 2 at 6.5 TeV, also thanks to smaller beam sizes from

2021 JINST 16 P03042

Table 2. Requirements for active halo control at the HL-LHC.

Parameter	Value or range
Transverse scraping range at 7 TeV [σ]	>3.6
Energy range for halo scraping, E_{min} [TeV]	> 5
Desired 90% tail scraping time [min]	5
Tolerated proton beam core emittance blow-up [µm/h]	0.05

the adiabatic damping at higher energy. On the other hand, beam measurements at this energy still indicated a large tail population in various phases of the operation cycle [26]. Recent concerns were brought up in association with a new effect observed in Nb_3Ti magnets, referred to as "flux jumps" [27], which is expected to trigger sudden field variations in the new dipole and quadrupole magnets at the HL-LHC, with subsequent transient beam variations. For a circular accelerator of the complexity of the HL-LHC, other effects causing beam losses might arise from sources yet unknown. The specifications of the HL-LHC HEL hardware, which are based on the experience obtained so far with transverse beam tail analysis, and the expected needs are summarized in table 2. The tolerated emittance blow-up is specified in [28]. The design is optimized for operation at 7 TeV, where the loss behaviour is most critical, although it is required to start tail control already during the energy ramp, in order to ensure the possibility to reach the top-energy plateau with the beam tails already under control. The phenomenon of flux jumps called for an assessment of the possibility to also use the HEL at lower energies. This aspect is discussed in section 4, where the electron-beam performance is described.

The experience with HEL collimation at the Tevatron [29] indicates that HEL is a very effective tool to mitigate issues related to transient beam losses, while remaining fully compatible with the standard operation of the collider. In the beam tests carried out at the Tevatron, suitable ranges of operational parameters could be found to improve the collimation performance with no visible deterioration of the luminosity. In particular, tail depletion resulted in reduced sensitivity to loss spikes in the presence of orbit jitters.

A key aspect in the decision-making process to include HELs in the HL-LHC baseline was the excellent experience obtained at the Tevratron with the HEL-collimation studies, carried out for the LHC in the framework of the US-LARP [30] programme. The Tevatron experiments on HEL-collimation were conducted on antiprotons, mainly at the end of regular collider stores. In some cases, the electron beam was turned on for the whole duration of the fill after collisions were established. Because of the flexible pulsing pattern of the high-voltage modulator [31], the electron beam could be synchronized with a subset of bunches, providing a direct comparison with the unaffected beam. The main results of HEL-collimation at the Tevatron can be summarized as follows [29, 32–34]:

- the use of HEL was compatible with collider operation during physics data taking;
- the alignment of the electron beam with the circulating beam was accurate and reproducible;
- the halo removal rates were controllable, smooth, and detectable;
- with aligned beams, there was no lifetime degradation or emittance growth in the core;

2021 JINST 16 P03042

- loss spikes due to beam-orbit jitter and tune adjustments were suppressed;
- the local effect of the electron beam on beam halo fluxes and diffusion speed were directly measured with collimator scans.

It is important to note that the operation at the Tevatron relied primarily on the use of DC electron beams, while for HL-LHC it is also planned to deploy pulsed-beam operational scenarios. These aspects are discussed in section 5. More recently, beam tests with hollow electron beams for collimation studies were also carried out at RHIC [35].

3.2 Operational conditions and electron beam requirements

The HEL produces an annular-shape electron beam that interacts with the circulating hadron beam over a distance of a few metres. The dimensions of the electron beam, specifically its inner radius r_i, which determines the smallest amplitude of halo particles affected by the active excitation, is defined by the constraint not to affect core particles while ensuring a sufficient range for depletion at amplitudes close to the primary collimator gaps. The smallest inner radius for halo control at the maximum LHC beam energy of 7 TeV was identified at 3.6σ, where $\sigma = \sqrt{\epsilon\beta}$ is the RMS beam size, for which we assume a normalized emittance $\epsilon = 2.5\,\mu$m. This ensures a clearance of about 3σ with respect to the nominal opening of 6.7σ the primary collimators in Pt7 [15].

Halo particles with amplitudes $A > r_i$ are affected by non-linear transverse kicks produced by the electron beam. The maximum kick θ experienced by a proton at radius r traversing a hollow electron beam enclosing current I_{er} in an interaction region of length L is given by the following expression:

$$\theta = \frac{1}{4\pi\epsilon_0}\frac{2I_{er}L(1 \pm \beta_e\beta_p)}{r\beta_e\beta_p c^2(B\rho)_p}, \tag{3.1}$$

where ϵ_0 is the vacuum permittivity, $v_e = \beta_e c$ is the electron velocity, $v_p = \beta_p c$ the proton velocity, and $(B\rho)_p$ is the magnetic rigidity of the proton beam. The '+' sign applies when the magnetic force is directed like the electrostatic attraction, i.e. when the electron beam moves in the opposite direction to the proton beam, whereas the − sign applies when the two beams move in the same direction. For example, in the HL-LHC configuration with $I_{er} = 5\,$A, $L = 3\,$m, $\beta_e = 0.237$ (corresponding to 15 keV electrons), $r = 2.2\,$mm, the corresponding kick is $\theta = 0.3\,\mu$rad for 7-TeV protons moving in the opposite direction to the electrons. The transverse cross section of the electron and proton beams at the HEL (left plot) and the dependence of the kick on the radial variable $r = \sqrt{x^2 + y^2}$ (right plot) are shown in figure 4, for the case of a cylindrical symmetry of the electron beam. Because of the betatron oscillations of the protons, the transverse kicks have different magnitudes at each turn and their strength is proportional to the electron-beam current and can be easily controlled. The particles in the core of the circulating beam (whose amplitudes are smaller than r_i) are — in the ideal case — unaffected if the distribution of the electron charge is axially symmetric.

Providing specifications for the HEL is a complex process, requiring various iterations over several HEL parameters, machine optics, and collimation system aspects, such as: (1) dimensions of the hollow cathode; (2) arrangement of solenoid fields of the HEL magnetic system; (3) optics parameters at the HEL location; (4) reference betatron cut of the betatron collimators in Pt7; (5)

2021 JINST 16 P03042

Table 3. Main parameters of the HL-LHC HEL.

Parameter	Value or range
Geometry	
Length of the interaction region, L [m]	3
Aperture of the proton-beam vacuum chamber [mm]	60
Inner solenoid cold-bore aperture [mm]	180
Outer cryostat diameter [mm]	≈ 500
Cryostat vessel pressure [bar]	3.5
Magnetic fields and magnet parameters	
Gun solenoid, B_g [T]	0.2–4.0
Collector solenoid [T]	0.2–0.4
Main solenoids (superconducting), B_m [T]	5
Range of compression factors, $\sqrt{B_m/B_g}$	1.1–3.75
Target compression factors	3.7 (0.375 T)
Electron gun and electron beam	
Inner/outer cathode radius, $r_{i,cathode}$, $r_{o,cathode}$ [mm]	4.0/8.0
Peak yield at 10 kV, I [A]	5
Maximum electron beam density [A/mm^2]	0.44
High-voltage modulator	
Cathode-anode voltage [kV]	15
Rise time (10%–90%) [ns]	200
Electron pulse duration [µs]	1.2–86
Maximum number of e-beam pulses per LHC turn	3

requirements of the main solenoid field to ensure stability of the electron beam. A critical element of the iterative process that led to the final specification of HEL parameters was the identification of the need for high output current cathodes of small transverse dimensions. As discussed in section 4.4, cathodes with inner radius $r_{i,cathode} = 4.0$ mm could be identified that provide an electron beam current in excess of 5 A. This value was assumed for a first definition of the HEL parameters. The initial assessment of the requirements on electron-beam stability indicated that, at the designated locations for the integration of the HEL (see section 2), a main solenoid field of $B_m = 5$ T is necessary along the straight path of the electrons. The local optical parameters were further optimized by increasing the β-functions in order to minimize the electron beam density for gaining further stability margin. Having defined these two parameters — $r_{i,cathode}$ and B_m — the rest of the required fields could be specified to achieve the desired electron beam compression for the interaction with the protons. The final values of the HEL parameters are listed in table 3, which includes also the specifications for the electron beam powering. The filling patterns of the LHC are built around bunch trains produced at the PS and then transferred to the SPS, with a 25 ns-spacing between bunches. A detailed description of these patterns is beyond the scope of this paper. It suffices to recall the main requirements that a filling scheme should fulfil and its features: each scheme must respect a 3 µs empty gap at the end of each 89 µs LHC turn for beam abort; the

2021 JINST 16 P03042

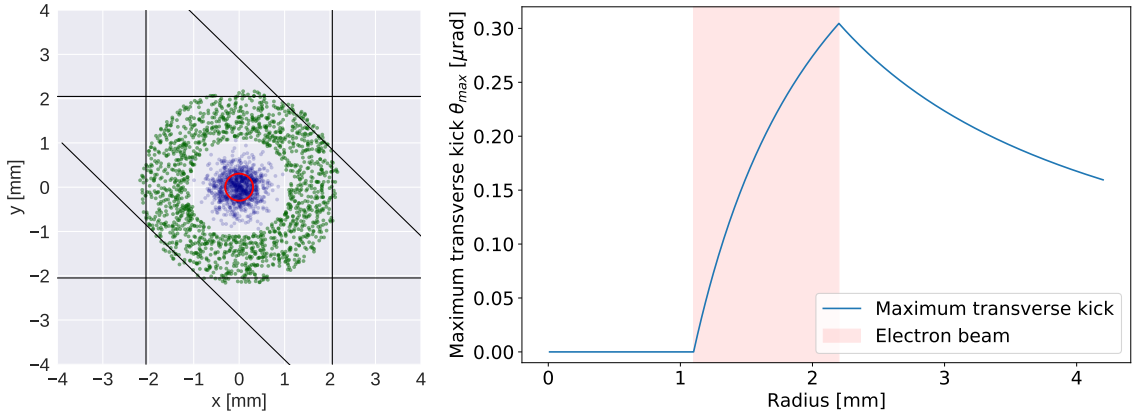

Figure 4. Left: transverse cross section with the beam distributions at the HEL: annular distribution of the electron beam (green) and Gaussian proton beam distribution (blue) with the 1 sigma envelope indicated in red. The black lines indicate the nominal 6.7σ opening of the three primary collimators (horizontal, vertical and skew), converted in mm at the HEL location. The reference optics of table 1 is used. Right: HEL kick experienced by a 7 TeV proton as a function of the radial coordinate.

minimum distance between LHC trains is about 800 ns, determined by the pulse duration of the injection kickers; within each LHC train, gaps up to 200 ns are present corresponding to successive injections into the SPS. This implies that for the HEL a rise and decay time of 200 ns is specified, in order to enable acting on sub-trains within a given LHC train. The duration of the electron beam pulses between 1.2 µs and 86 µs allows an ample flexibility in acting on different types of bunches and trains.

The main requirement for the HEL is to provide adequate halo scraping at top energy, both for proton and ion beams, when beam losses are more critical for the machine. One requires to be able to switch the HEL on during the energy ramp above 5 TeV (see table 2) such that the top energy can be reached with tails already depleted. Halo removal at much lower energies might be inefficient because tail-population mechanisms in the ramp might induce a strong generation of beam halo. Hence, in normal conditions, tail scraping should not start earlier than strictly needed.

No specific loss problems are expected at injection energy, but the possibility to use HELs at 450 GeV is considered as a key asset for an efficient commissioning of these complex devices, e.g. with smaller-than-nominal emittance beams or with specially tuned optics, designed for smaller values of the β-functions at the HELs locations. Note initial beam commissioning and HELs setup can be performed more efficiently at injection energy, avoiding the long full LHC operational cycle. Typically, a 2 h turnaround time is expected to be needed to recover the top-energy conditions after a beam dump at 7 TeV, if one operates at top energy only, while at 450 GeV, subsequent beam injections can be obtained within minutes.

Recently raised concerns with the flux jumps in the new HL-LHC magnets [27] required assessing the use of HELs below 5 TeV. The maximum value of sigma at which one can start cleaning the beam halo for the largest inner electron-beam radius achievable is shown in figure 5. This is computed as a function of the proton-beam energy, assuming a constant electron beam size at a compression factor of 1.1. The HEL design allows, for example, cutting the tails at 4.5σ at

2021 JINST 16 P03042

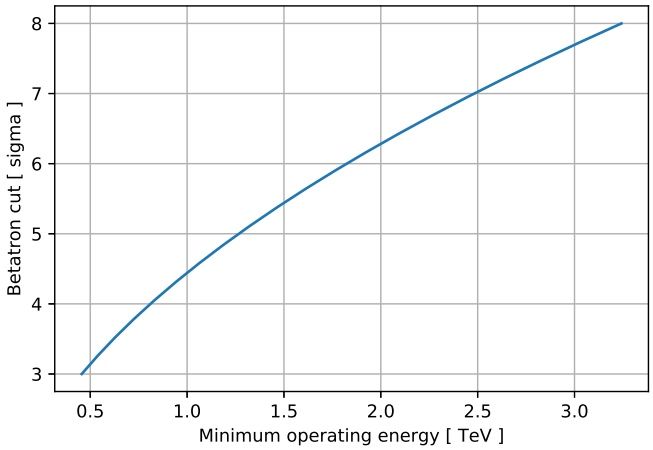

Figure 5. Achievable betatron cut as a function of the proton-beam energy with the minimum electron beam compression factor of 1.1 (see table 3). Realistic operational scenarios, e.g. cut of the order of 4.0–4.5σ are within reach already for beam energies smaller than $\approx$ 1 TeV. Operations at injection are quite aggressive, though, and only compatible with commissioning tests, as it is not planned to clean down to 3σ the full beam at injection.

beam energies of about 1 TeV. The maximum cut at 450 GeV is about 3.0σ that is probably too tight for operation at high intensity, but can be used for HEL commissioning scenarios at injection, as introduced above.

4 Design of the HL-LHC lenses

4.1 Overall design

The overall design of the HL-LHC HEL is shown in the 3D view in figure 6. A cut view showing the cross section of the key components is given in figure 7. The design is based on superconducting magnets operating at 4.5 K. The magnet system is built around a warm vacuum chamber with a 60 mm inner diameter and is designed to steer and stabilize a 5 A, 15 keV electron beam that interacts with the proton beam over a distance of 3 m. The 5 T solenoid field in the HEL straight section is produced by two identical magnets, with a gap in between for beam diagnostic purposes (see section 4.5). Tilted solenoids located at both sides of the main ones are used to steer the electron beam on, and out, of the proton beam.

An S-shape design, with electron beam generation and disposal systems located at opposite sides of the proton beam, is adopted for the HL-LHC. Contrary to the U-shape design adopted in other colliders, like the Tevatron [19] and the RHIC [36], the HL-LHC design ensures a self-compensation of asymmetries in the electromagnetic fields experienced by the circulating proton beam at the entrance and exit of the electron beam. This is important to minimize the effect on the beam core of the pulsed-beam operation needed at the HL-LHC. A disadvantage of this design, however, is that the transverse component of the magnetic field generated by the two steering

2021 JINST 16 P03042

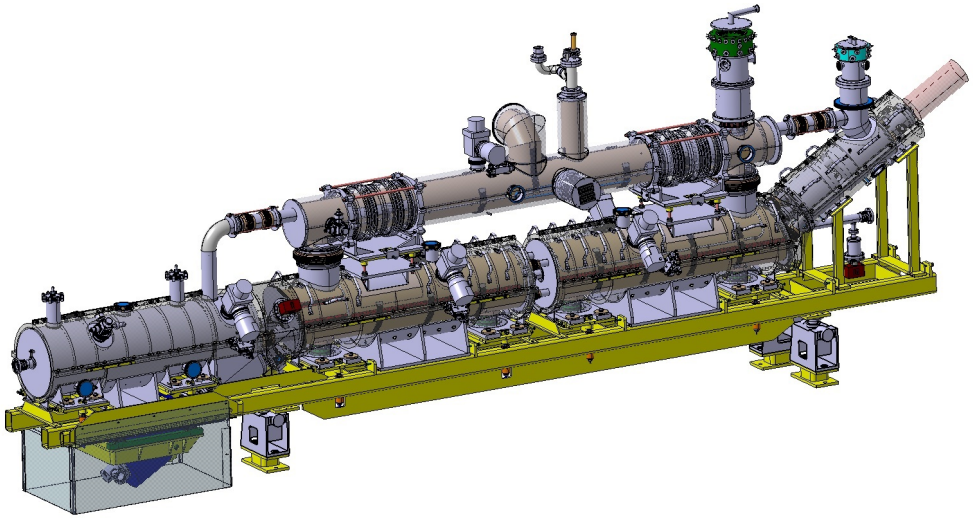

Figure 6. Design of the HL-LHC hollow electron lens. The gap between the two main solenoids houses diagnostics not shown in this figure (see section 4.5).

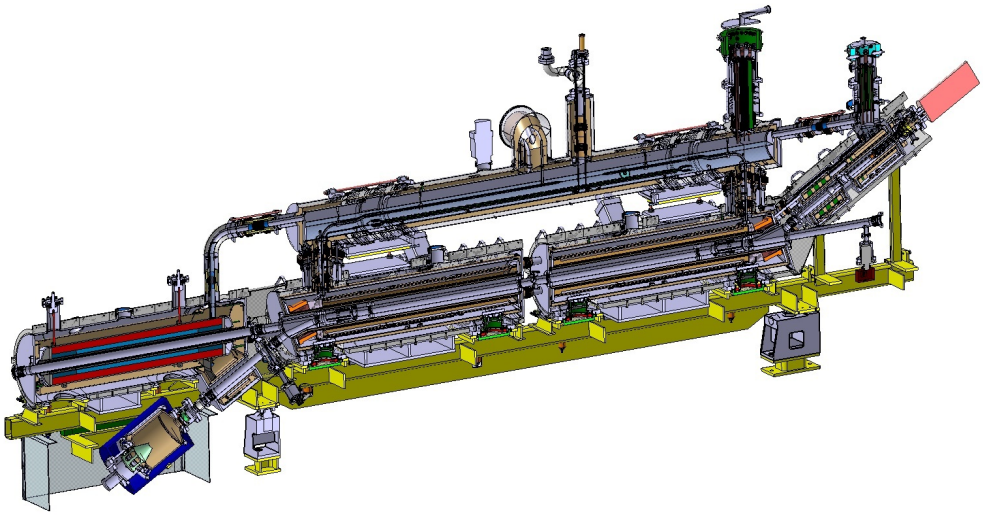

Figure 7. Cross section of the HEL showing the key sub components.

solenoids adds up and results in a net vertical kick for the proton beam. This requires a dipole magnet (visible on the left side of the drawings in figure 6 and figure 7) that compensates this kick.

4.2 Magnet system

The magnetic system for the electron beam stabilization, adiabatic magnetic compression, transport, steering, and optimization is one of the key components of the HEL. The HEL magnet system is housed in a cryostat designed to operate at a nominal pressure of 1.3 bars, compatible with a maximum of 3.5 bars, (see section 4.3) and to use 4.5 K saturated liquid helium II.

2021 JINST 16 P03042

Table 4. Main parameters of the HEL magnets.

Super-conducting magnet	Main solenoid	Correctors		Compensator
Magnetic field orientation	Axial	Horizontal	Vertical	Vertical
Number of magnets	2	7	7	1
Inner coil radius, mm	90	125	120	61
Outer coil radius, mm	111	129.4	124.4	73
Coil length, mm	1500	488	488	≈ 1000
Layers number	20	4	4	2
Turn number/layer	909	24	24	8
Total turn number	18180	96	96	150
Operating current I, A	330	120	120	220
Central field, T (self)	5	0.08	0.08	0.74
Stored energy, kJ	455	0.053	0.053	2.8
Inductance, H	7.73	0.00739	0.00734	0.115

The most demanding magnet is the 5 T main solenoid, with a 180 mm inner bore diameter, split in two sections of 1.5 m length (see figure 6) to allow some space at the centre of the straight interaction region for diagnostics as well as to reduce the individual magnet stored electromagnetic energy to less than 500 kJ. The strong magnetic field in the straight section of the HEL assures that a small electron beam size and optimal electron beam stability can be achieved through fast Larmor oscillations around magnetic field lines. The requirement of the straightness of the solenoid field lines is set to $\Delta_{x,y} \approx 0.15$ mm, and allows preventing deviations of the electron beam trajectory larger than a fraction of the proton transverse beam size. This imposes a very small relative transverse field deviation of 10^{-4}.

Two tilted solenoids are used for the e-beam bending, and the sum of their vertical kicks is cancelled by the dipole compensator installed at the collector side of the HEL (see figure 6). The compensator reaches integrated dipole fields up to 0.4 T m. The HEL design includes the ability to adjust the electron trajectory to the straight line of the proton orbit using the upstream position (controlled by gun correctors) and angle corrector along the main solenoids, in both horizontal and vertical planes. The strength requirements of each of the six longitudinal individual dipole correctors is currently set at 0.125 T mm/A with a self peak field at 76 mT that allows moving the electron beam trajectory by ±3 mm in the 5 T main solenoid field. The list of other smaller circuits for the electron beam steering is given in table 4.

The gun solenoids require a maximum design current of 320 A for a peak field of 4.5 T that can be tuned in the 0.2–4 T field range as function of the energy of the proton beam, achieving an adiabatic compression ranging between 1.1 and 5, with the target value of 3.7 (see table 3). An illustration of the planned circuit scheme is given in figure 8, with the types of planned power converters and the circuit protection approach. Dedicated energy extraction systems are planned for the quench protection of the main solenoids, of the gun and bending solenoids and of the dipolar orbit compensator (blue in figure 8). The other circuits do not require energy extraction.

The solenoid coils are made of a rectangular insulated Nb-Ti conductor wires with insulated dimensions of 1.65×1.05 mm^2 (filaments in copper matrix) The insulation thickness is 0.02 mm.

2021 JINST 16 P03042

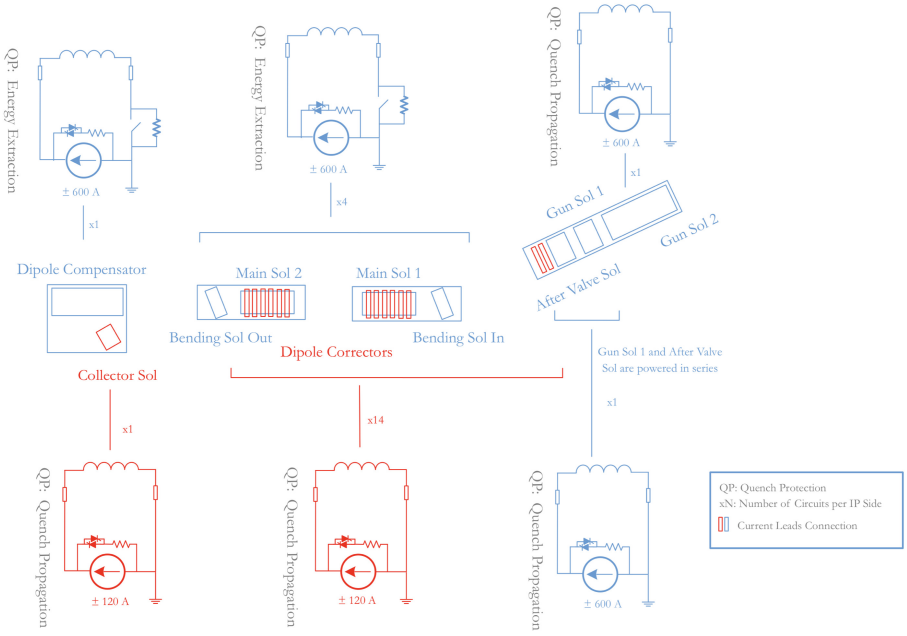

Figure 8. Circuit overview for the present HEL magnetic system. *Courtesy of S. Yammine, CERN, for the Magnet Circuit Forum (MCF).*

The wire has a 805 A critical current at 4.2 K and 5 T and a Cu/super-conductor surface ratio of 4. The packing factor is 0.85. The cable shall be wrapped in a polyimide film of an equivalent 0.03 mm thickness. It is expected that the final insulation details shall be fixed with manufacturers.

The total stored energy in the solenoids is about 1.1 MJ. The results of a simulation of the quench process in the coils of the main solenoids show that, after the quench detection and after switching off the power supply, one can allow most of the energy to be dissipated in the coil and a fractional amount of up to 15% into the energy extraction dump resistor in less than 2 s. In this case, the temperature of the hottest spot in the coils will be kept below 120 K. Details of the quench protection system are being finalized.

4.3 Cryogenics system

From the point of view of the integration in the LHC cryogenics system, the HEL is comparable to the stand-alone magnets that are used in the matching sections in the various LHC points [1]. The HELs will be cooled at 4.5 K and one of the driving arguments to install them in the LHC straight section around Pt4 is the availability of an adequate cryogenic system in this area that can be adapted to the HEL needs.

From the cryogenic point of view, the different solenoid magnets and correctors are installed in a vacuum-insulated cryostat and immersed in a bath of saturated liquid helium at 4.5 K. Different cryostats, all connected to the same cryogenic distribution line, are needed (see figure 7): (1) a central one, split in two, includes the main solenoids, the tilted steering solenoids and the corrector magnets in the straight part; (2) one for the gun magnet and its corrector magnets; (3) one for the dipole compensator and the collector solenoid (see also figure 10). All the superconducting

2021 JINST 16 P03042

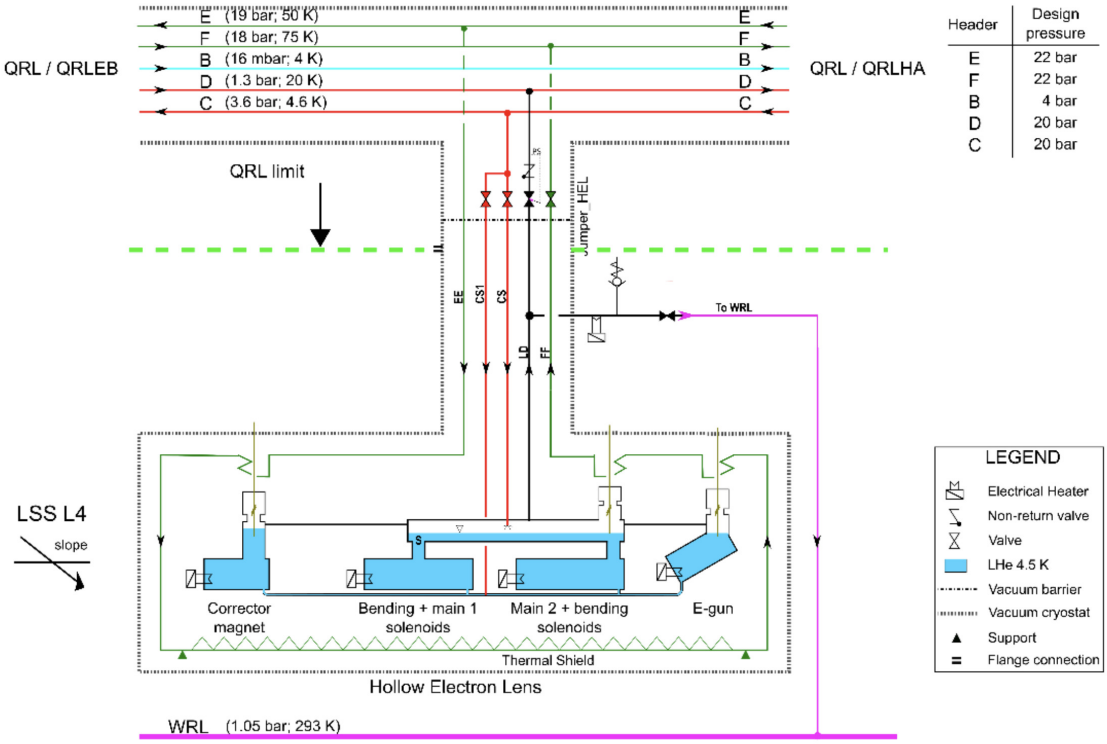

Figure 9. Schematic view of the cryogenic distribution lines planned for the HEL.

magnets are electrically fed with the so-called conduction-cooled current leads. Figure 9 shows the current cryogenics circuit scheme and connections to the cryogenic ring line (QRL) of the LHC [1].

The main feeding line (called header C) provides super-critical helium, which is expanded in a Joule-Thomson valve. The expanded helium line (CS line) feeds the cryostats with saturated liquid helium. The helium gas, resulting from the expansion of the pressurized liquid helium, is recovered via a gas collector, which is itself connected (Line D) to the QRL header D used to recover cold gas from all other devices in Pt4. The line D protects the cryostat from any pressure back-filling by using a combination of a valve, a check valve and a pressure switch. During the cool-down phase, a parallel second feeding line (Line CS1) will be used to control the temperature gradient of the cryogenics magnets.

A thermal shield circuit is also foreseen. This circuit is connected with the QRL and is used also as thermal intercept of the conduction cooled current leads. A regulation valve controls the outlet temperature. The design of the cryostat allows a maximum pressure of 3.5 bar. A pair of safety devices will protect the helium circuits at this level of pressure. The total helium inventory is at about 40 kg of liquid He at 4.5 K under stable conditions (4.5 K, 1.25 bar).

4.4 Electron-beam generation and disposal

The cross section of the HEL transitions dedicated to the electron beam injection in and extraction from the region of interaction with the proton beam is shown in figure 10. The HEL gun and collectors are evidently part of the primary LHC vacuum and thus particular care must be taken to ensure that they are properly conditioned prior to hadron-beam operations, and that in all operating

2021 JINST 16 P03042

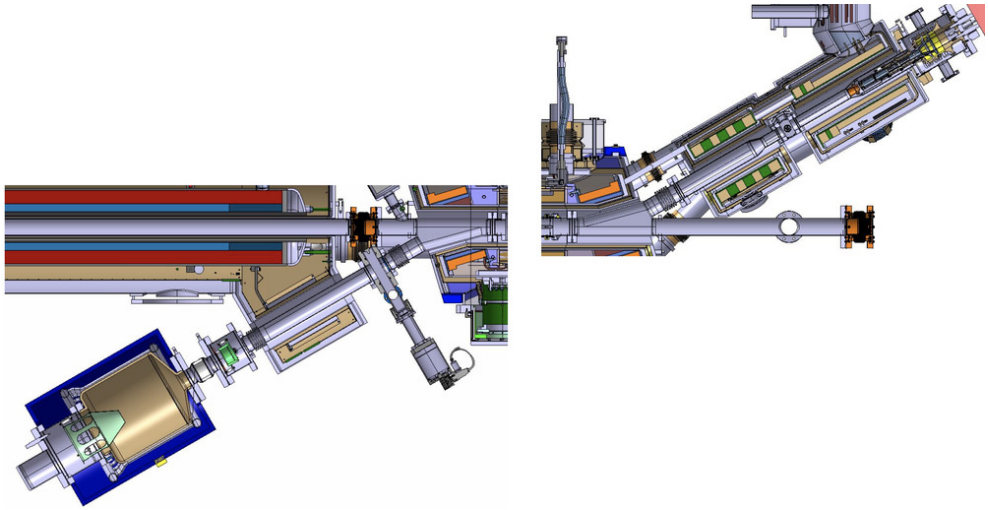

Figure 10. Cross section of the transitions at the incoming (right) and outgoing (left) sides at the electron beam path.

scenarios they do not compromise the beam performance from the vacuum point of view. For possible replacements of the gun during early technical stops or — if unexpectedly needed — during the run, vacuum valves are planned immediately downstream of the gun solenoid and upstream of the collector, just at the end of the straight interaction region between protons and electrons.

The 3D drawing of the thermionic gun is shown in figure 11. The development of high current-density cathodes is important for the HL-LHC HEL in order to keep reasonably moderate magnetic compression factors while aiming at small electron beam sizes. Details of the gun developments are discussed in a companion paper in this newsletter [37]. Initial designs for the HL-LHC HELs gun started from the state-of-the-art gun developed at Fermilab for collimation studies, under the scope of US-LARP and relied on a cathode with a 6.75 mm inner radius that was tested extensively [38]. The present HL-LHC design uses a new, smaller cathode made of impregnated scandate, developed by Beijing Vacuum Electronics Research Institute (BVERI) in collaboration with CERN. The cathode has a 4.05 mm inner radius and a 8.05 mm outer radius, and is capable to deliver current densities larger than 0.4 A/mm, exceeding the 5 A target output current with a 10 kV extraction voltage, at an operating temperature of about 900 degrees.

The cathode lifetime should be sufficient to ensure at least one full year of operation of the HL-LHC without replacements. Assuming the typical figure of about 200 days of operation per year [28], one requires a lifetime of about 5000 hours. This figure is quite pessimistic as it assumes continuous operation of the cathode. Note that the cathodes being developed for the HL-LHC have been tested during 10000 hours without significant performance degradation and thus fulfil the HL-LHC requirements. In fact, it is expected that they might be operated for several years without replacement, assuming a realistic figure of $\approx$ 50–60% duty factor if, for example, HEL are used continuously only during the collision process.

The gun design is shown in Figs 11 and 12. Compared to the initial design, it has been made significantly more compact in order to simplify the design of the superconducting solenoids at the electron beam generation that surround the gun [37]. A longer structure than in the initial design is

2021 JINST 16 P03042

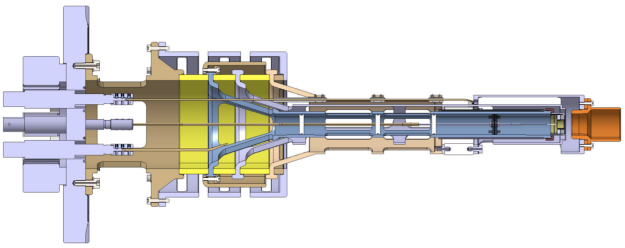

Figure 11. Cross section of the HL-LHC thermionic gun, optimized for the small cathode design with outer radius of 8.05 mm, from [37].

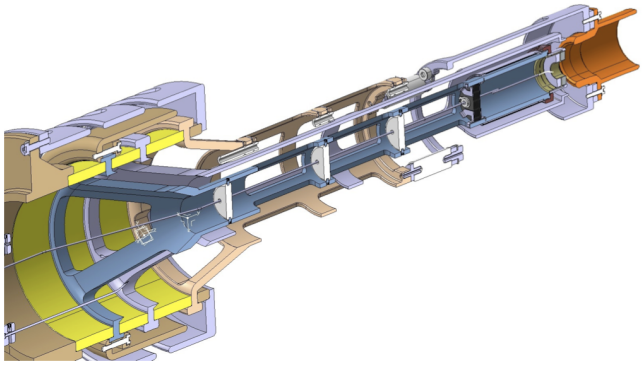

Figure 12. 3D view of the HEL gun.

adopted in order to position the cathode in the longitudianl centre of the gun solenoid. The design of the ceramic parts (see yellow rings in figure 12) and connections have been optimized in order to maximize insulation and heat exchange. This will avoid overheating of the ceramic while the cathode is kept at its operating temperature, which in previous designs had caused vacuum concerns. Tests with a final prototype based on this design are expected by mid 2021.

The electron beam collector is shown in figure 13. It is designed to sustain, without damage and with limited temperature increase, a continuous operation of the electron beam at 15 kV in DC mode, for a total power of 75 kW. This criterion is very pessimistic, as electron beam simulations [39] indicate that at maximum current, the electron beam energy is not expected to exceed 12 keV, for a maximum of 60 kW. Furthermore, it is planned to bias the electrodes at the entrance of the collector, to reduce the energy deposited to the collector, the secondary electron emission (therefore maximizing the electron efficiency) and the gas induced desorption (to guarantee best vacuum performance). Engineering margins on the design are being finalized, taking into account that the duty factor in operation might be significantly lower than unity for several considered powering schemes [40] and that the possibility to add a bias voltage to decelerate the electron beam before it reaches the collector is planned.

The components exposed to the beam are made of copper, which is water cooled through the scheme shown in figure 13. A small solenoid is added at the end of the electron path, downstream of the vacuum sectorization valve and just upstream of the collector (see left graph in figure 10). It maintains small beam sizes in the aperture-critical transition region and equalizes the distribution at the exit with respect to the incoming beam, for optimum compensation in the S-shaped design.

2021 JINST 16 P03042

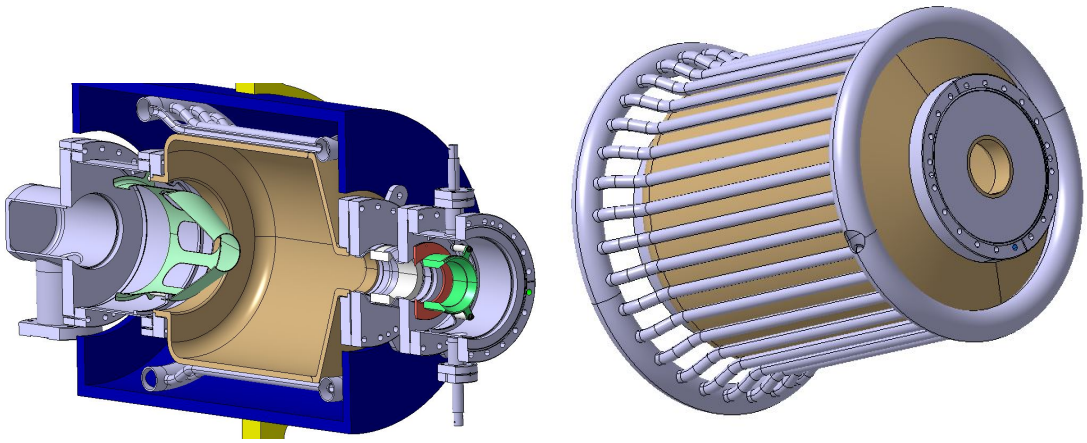

Figure 13. Design of the HEL collector: 3D view of the full assembly (left) and detail with the piping for the water cooling system (right). The conical component at the end of the collector (light red) is a barrier electrode that prevents electrons reaching the downstream vacuum equipment.

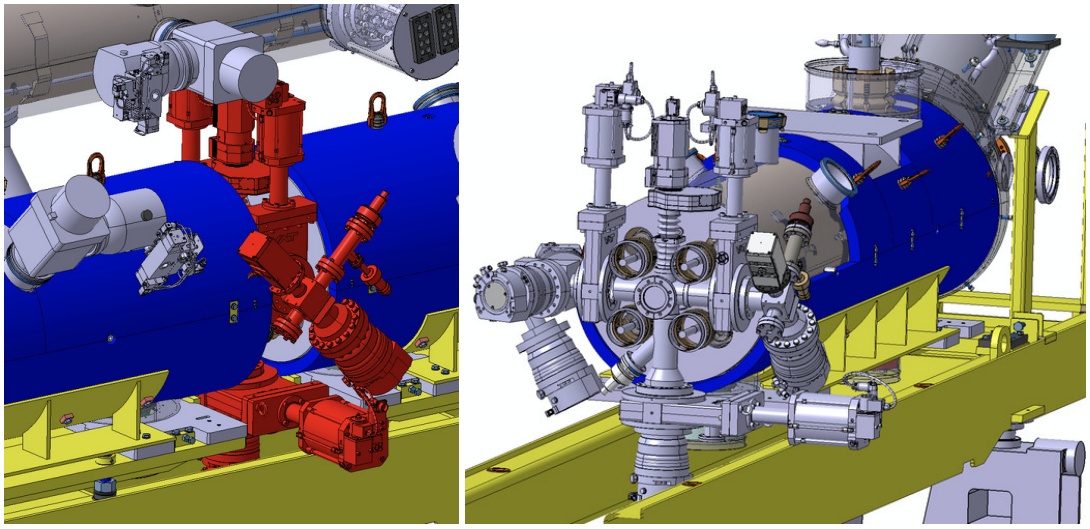

Figure 14. Preliminary design of the BGC monitors installed in the middle of the HEL, between the two main solenoids, to measure at the same time 2D profiles of the proton and electron beams: 3D view showing the integration between the magnet cryostat (left) and cut view of the transverse cross section (right). *Courtesy of I. Papazoglou and G. Schneider, CERN, SY-BI.*

4.5 Electron-beam instrumentation

The operation of the HEL relies on a novel beam gas curtain (BGC) monitor, developed to measure at the same time the transverse profiles of the hadron and electron beams and feedback on the relative centring of the two beams. This instrument relies on the fluorescence induced by the beams interacting with the gas. A nozzle is used to inject at high-speed a thin sheet of gas — the "curtain" — in the middle of the HEL. The current integration of this instrument is shown in figure 14. The appropriate gas species to be used is still being discussed, and the final choice (between Neon or Nitrogen) will follow tests with proton beam that are planned in the LHC Run 3.

2021 JINST 16 P03042

Two Beam Position Monitors (BPMs) per HEL are foreseen to be placed at the beginning of the first main solenoid and at the end of the second. They will measure the position of both electron and hadron beams, and the angle between the injection and extraction of the electron beam. Efforts are being made, by investigating both the BPM design and the modulation scheme, to be able to use the same electronics for both electron and hadron measurements, so to provide a good accuracy in the relative position and assist the steering of the electron beam injection. The type of BPM selected is a strip-line type, given its higher sensitivity to low frequency signals. Efforts are being made, by investigating both the BPM design and the modulation scheme, to be able to use the same electronics for both electron and hadron measurements, so to give a good accuracy in the relative position and assist the steering of the electron beam injection.

In addition, one beam loss monitor (BLM) will be installed for each HEL device. No local hadron-beam losses are expected to be caused by the HEL itself, since the small kick experienced at each passage by the halo particles causes an enhanced diffusion that translates into losses at the Pt7 primary collimators. The BLMs are used to protect the HEL, and will detect unexpected local beam losses on the HEL aperture, avoiding accidents by triggering a hadron-beam abort if pre-defined loss thresholds are exceeded.

The HL-LHC upgrade also includes the installation of two coronagraph devices [41] for the measurements of beam halos. These instruments use the LHC synchrotron light telescopes to measure beam-halo populations at a level of 10^{-5}. During the 2015-2016 winter shut-down period, one of the two LHC synchrotron light monitor systems was equipped with a prototype beam-halo monitor, based on the Lyot coronagraph, classically used in astrophysics telescopes to observe the sun's corona. This first prototype has been designed as a demonstrator system aimed at resolving a halo-core contrast in the range 10^{-3} to 10^{-4}, with the final aim to achieve 10^{-5}. This instrument will be able to resolve the beam halo scraped by the HEL and provide feedback on its operation.

4.6 Tunnel integration

The integration aspects of the installation of the HEL in the LHC Pt4 were addressed in detail early on in the project. Finding adequate space for these new devices, including what is required for services, was evidently one important step prior to the inclusion of this item in the HL-LHC baseline. The final longitudinal positions were introduced in section 2. The present 3D views of the two HEL locations for Beam 1 and Beam 2 are shown in figure 15, top and bottom panels, respectively. The HELs are installed close to the "dogleg" dipoles in Pt4, on the IP4-side where the inter-beam distance is at its maximum value of 420 mm [1]. The orientation of the two HELs is mirror-symmetric on the left (Beam 1) and right (Beam 2) sides of the IP4, as the electron beams travel on the opposite direction of the clockwise Beam 1 and anti-clockwise Beam 2.

5 Expected performance

Let us define the beam halo as the fraction of the circulating beam above r_1, while the beam core is represented by the portion of circulating beam surrounded by the electron beam. The HEL performance is defined by the combination of halo removed and side effects on the beam core, i.e. the larger the fraction of halo removed without inducing a beam-core blow-up, the better the HEL performance.

2021 JINST 16 P03042

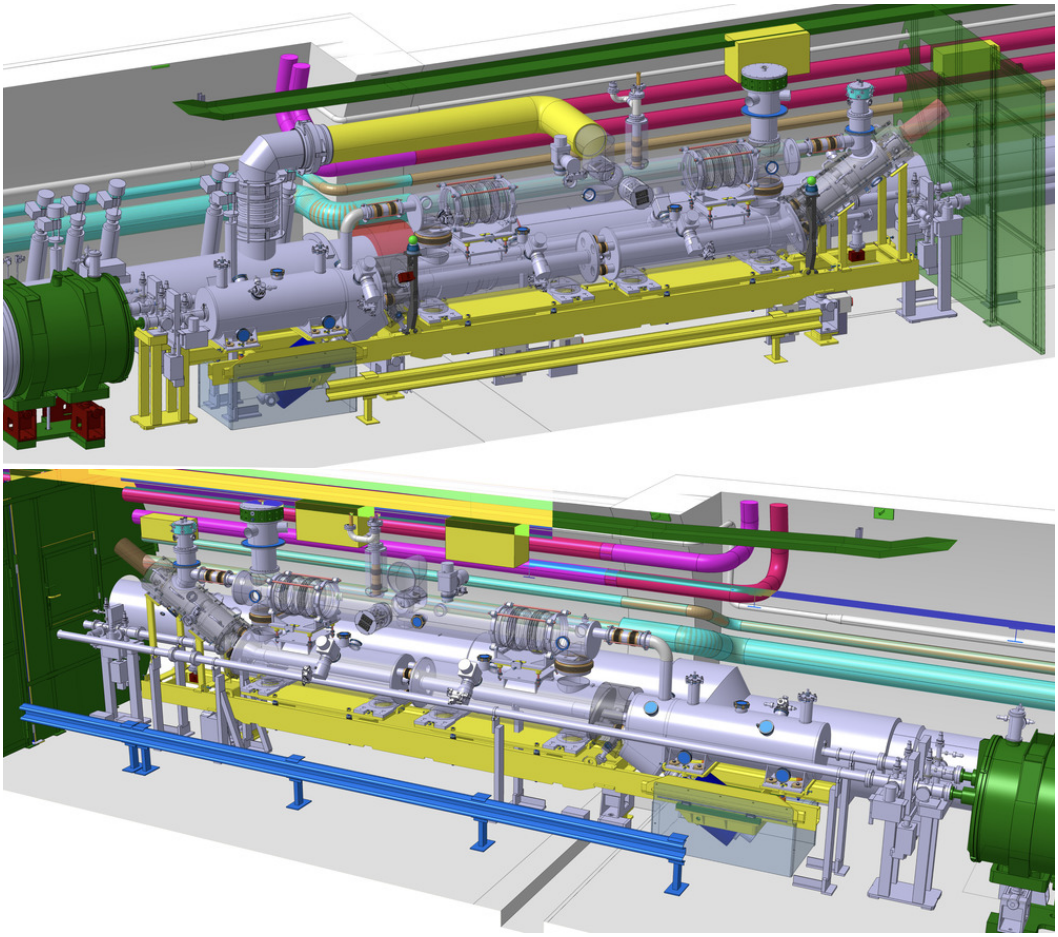

Figure 15. Integration drawings for the HEL of Beam 1 (top, left side of Pt4) and of Beam 2 (bottom, right side of Pt4). Both lenses are installed immediately downstream — along the beam direction — of one of the two dogleg dipoles (red in the figures) that increase the inter-beam distance from 194 mm to 420 mm [1]. *Courtesy of J. Oliveira and P. Fessia, CERN, ATS-DO, for the HL-LHC WP15.*

The HEL performance assessment relies on multi-turn tracking simulations carried out with `SixTrack` [42–46] that allows a symplectic, fully chromatic, and 6D tracking along the magnetic lattice of the machine, taking into account interactions with the ring collimators and the detailed aperture model of the entire ring. The code has been compared to LHC data in a number of studies [4, 7, 11, 47–50] with excellent agreement. HELs are integrated in the lattice as magnetic elements [51, 52] and their effect on the beam can be modelled using different electron beam kicks (earlier studies can also be found in [53, 54]). Dynamic Aperture (DA) simulations and Frequency Map Analysis (FMA) are faster than complete halo-depletion simulations. Thus, DA and FMA studies were initially carried out to explore the available parameter space of relevant parameters (machine configuration in terms of chromaticity and Landau octupole settings, electron-beam parameters) and to guide the choice of a subset of promising HEL configurations. Then, detailed estimates of tail depletion and estimates of the impact on the core were derived for these selected subsets of cases only. A complete overview of the results obtained is reported in [40] and goes beyond the scope of this paper. Nevertheless, the main conclusions that can be drawn from

2021 JINST 16 P03042

those studies are reported below. Earlier simulations of the effects on the core and experiments in the LHC using the transverse feedback system to mimic the residual kicks of an electron lens were published in ref. [55].

5.1 Electron-pulse patterns

The electron beam can be switched on and off with different patterns on a turn-by-turn basis determining the effect on both core and tails of the circulating beam distribution. Possible modulation structures that have been considered are:

- *Continuous* (DC): the electron beam is switched on at every turn with the same electron beam current (it is nevertheless switched off in the abort gap, as mentioned in section 3.2).
- *Pulsed* (P^i_j): the electron beam is switched on with a given current for i turns and then off for j turns.
- *Random* (R_p): the electron beam is randomly switched on for one turn with a probability $p \in (0, 1)$. The current if the HEL is switched on is the same for the different turns.
- *Random current* (R_I): the electron beam is switched on at every turn, but the current is randomly changed on a turn-by-turn basis according to a uniform distribution of values between 0 A and 5 A.[1]

Examples showing the excitation profile in time for the different schemes are reported in figure 16. Note the pulsed pattern R_I is the most challenging from the hardware point of view, and, although other patterns featuring changes of electron beam current could be envisaged, one of the main aims is to identify the best compromise between required HEL performance and hardware feasibility. Also, note that the duration of the electron pulses can be adjusted to cover a different number of HL-LHC bunches (see table 3) but this has no effect in these studies that are done for single bunches (real machine losses will have to be scaled according to the number of excited bunches).

5.2 Halo-depletion

The most efficient mode of operation is R_p thanks to its spectral content (white noise). This means that resonant kicks are given to all particles above r_1, enhancing their diffusion speed towards primary collimators. On the other hand, this implies that resonant kicks are given also to the beam core if the residual field is non-zero, possibly leading to a significant emittance blow-up, as discussed in section 5.3. Studies were performed to define margins on both the electron beam current and the probability to be switched on at each turn, which can provide a very useful mitigation measure in case of limitations on the current delivered by the electron gun, power deposition on the electron collector, or large residual field on the beam core [40]. An almost complete halo removal after about 100 s is expected using the pulse $R_{0.5}$ with 5 A electron beam current and $r_1 = 5\,\sigma$, as shown in figure 17a. The random excitation remains effective also at lower electron beam currents. For

[1] Previous studies, see for example [53], considered a similar excitation based on turn-by-turn variations of the electron beam current, modulated at frequencies close to that of the betatron tune. The study reported here explores only the random mode. It has been assessed that fast, turn-by-turn changes of the electron beam current are complex at the frequencies of interested so, as discussed below, the interested will be focused on *Pulsed* and *Random* modes.

2021 JINST 16 P03042

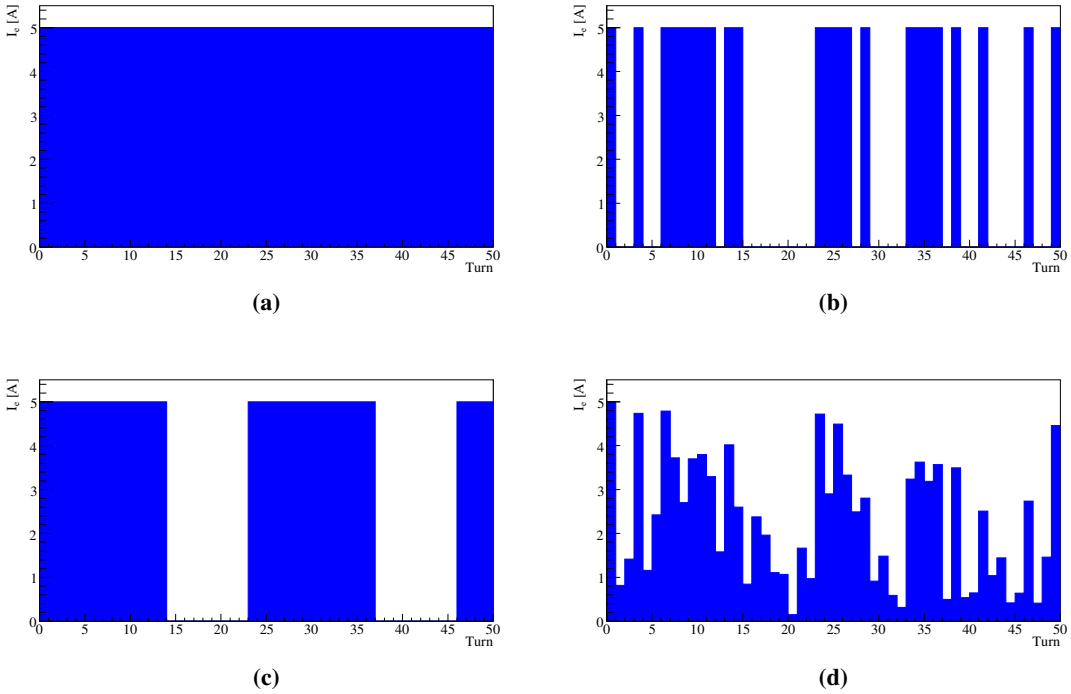

Figure 16. Examples of HEL pulsing pattern: (a) DC, (b) $R_{0.5}$, (c) P_9^{14}, (d) R_I

example, operating the lenses with this pulsing scheme but at currents 2–3 times lower than the 5 A design value could be a likely scenario to mitigate effects on the core in case of residual fields.

A generalized approach in the definition of a deterministic pulsing pattern allowed identifying the innovative and promising pattern P_9^{14}, which could significantly enhance halo removal performance with respect to the DC excitation, as shown in figure 17a.

The halo depletion with the pulse R_I is equivalent to the one obtained with $R_{0.5}$ and $I_e = 3$ A, indicating that from the halo removal point of view there is no need to search for complex hardware solutions to make the pulse type R_I feasible [40].

5.3 Impact on beam core

The initially estimated residual kick in the centre of the hollow electron beam is about 5 nrad and below 0.1 nrad in the vertical and horizontal planes, respectively [56], with the current HL-LHC HEL design. This is prior to a final optimization of the magnetic system design [39]. Hence, only the vertical residual kick was simulated, being the dominant contribution. Note that the acceptable continuous emittance blow-up in HL-LHC is below 0.05 µm/h [28].

A negligible emittance growth is found for the pulses DC and P_9^{14}, as shown in figure 17b, within the error estimated for a simulation time of 1000 s. On the other hand, an emittance blow-up of a factor about 100 larger than the tolerated one is observed for the pulse $R_{0.5}$, even if the strength of the residual kick is reduced to 1 nrad. The growth is visible only in the vertical plane, as expected because in these simulations the linear coupling is perfectly corrected. Effects of a realistic linear coupling correction are discussed in detail in [40].

2021 JINST 16 P03042

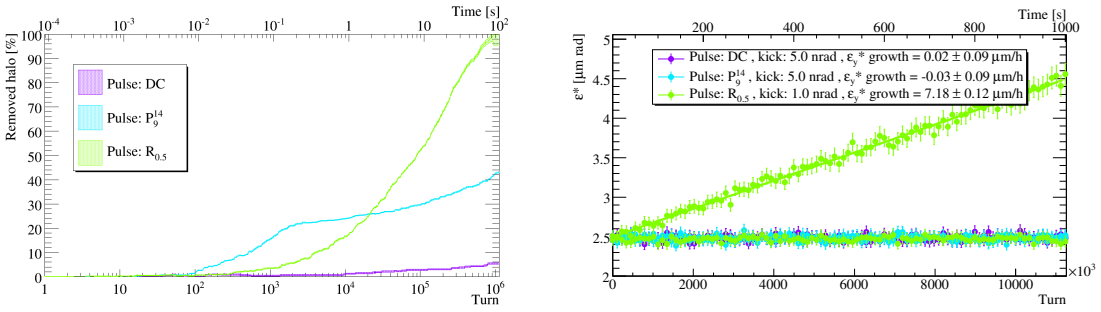

Figure 17. (a) Estimate of the expected beam halo removal after 100 s for various HEL pulsing pattern. (b) Emittance evolution for different HEL pulse patterns. Solid and dashed lines represent the expected trend in the vertical and horizontal planes, respectively.

It is important to find possible mitigation strategies to enable the use of R_p, as it provides the best halo removal performance. Thus, parametric studies were carried out, also with the aim to provide input on required magnetic design quality and the maximum acceptable residual kick on the beam core.

Margins on electron beam current and on probability to be switched on have been exploited and combined with the effect of the transverse active damper (ADT) that is present in the LHC [57]. An optimized HEL magnetic design with a residual kick below 3 nrad would make even a continuous use of R_p possible when the beams are not colliding [40], according to our simulations. On the other hand, when beams are colliding the tune spread is dominated by head-on beam-beam, which reduces significantly the emittance-growth suppression achievable using the ADT, essentially making it impossible to use the R_p pulse. The use of the DC pulsing is demonstrated in all cases to have negligible effects on the core over long times and is being considered for continuous operation during collisions in case of unexpected effects when using other excitation modes. Note that the DC powering was also the operational mode adopted successfully in hollow electron beam tests at the Tevatron [29].

5.4 Next steps on HEL performance studies

Some additional factors must be taken into account to refine the possible operational scenarios that have been defined for the use of HEL in HL-LHC, such as pulse-to-pulse stability of the electron beam, linear coupling, and dependence on the betatron tune, which goes beyond the scope of this paper and can be found in [40].

Of course, the HL-LHC operational cycle, lattice and optics configurations are still evolving [21]. On the other hand, no significant changes are expected for non-colliding beams in the overall results presented here, because strong non-linearities are present in the lattice used, which are the main driving term of HEL performance. The tune footprint is significantly affected by head-on beam-beam and certainly one imminent follow up is to demonstrate the effectiveness of the DC and P_j^i pulsing schemes taking beam-beam effects into account.

2021 JINST 16 P03042

6 Conclusions

Hollow electron lenses will be installed in the LHC in the long shutdown 2025–2027 as part of the HL-LHC project. Together with other upgrades of the collimation system, they are designed to improve the performance of the HL-LHC, which aims at doubling the LHC design stored beam energy. The HL-LHC HELs are designed to enable efficient cleaning of beam tails of the ultra-high intensity hadron beams planned for the HL-LHC. High-current electron beams, with different possible pulsing patterns, are used to dispose of halo particles in a controlled way, which otherwise will populate the phase space close to the aperture of the primary collimators of the betatron cleaning system. These large-amplitude particles do not contribute significantly to the luminosity performance of the collider, but pose a significant threat to the availability of the accelerator: loss spikes might be induced by small shifts of the circulating beam orbit and machine equipment might even be put at risk of damage in case of fast beam losses.

The HL-LHC HELs are designed to provide high current-density electron beams with inner radius as small as 1.1 mm and maximum design current of 5 A. These beams are steered and stabilized thanks to a complex system of superconducting magnets, based on 5 T main solenoids and various other smaller solenoids and dipole correctors. Different time profiles for the electron beam powering are possible, offering a large flexibility to act on the variety of beam filling schemes considered for the HL-LHC.

The DC powering mode for the electron beam, possibly pulsed in the abort gap or between trains depending on the number of bunches that the HEL needs to act on, is fully transparent for the circulating beam core. This is the case even in the presence of a residual field in the hollow electron beam centre. On the other hand, our simulation studies raised the concern that this DC mode might not provide sufficiently fast tail depletion rates in all required operational scenarios, and specifically with non-colliding beams at top energy. Other pulsing schemes have therefore been studied considering different turn-by-turn modulations. These risk to cause core emittance blow up for non-ideal hollow beams, where the field in the centre of the annual electron distribution is non-zero. Various pulsing schemes were investigated in simulations to mitigate this risk. Our study allowed devising operating schemes with minimum risk to induce beam-core emittance blow up. The study will continue and be extended to the case of colliding beams. At the same time, the hardware must be optimized to minimize the residual field experienced by the hadron beam core. A preliminary threshold for the acceptable residual dipole field was defined for the most aggressive powering schemes.

These studies will be used to finalize the overall design of the HL-LHC HELs. It is currently planned that these devices will be built at the Budker Institute for Nuclear Physics (BINP) as an in-kind contribution to the HL-LHC project.

Acknowledgments

This work is supported by the HL-LHC project.

The authors would like to sincerely acknowledge the contribution of various colleagues at CERN and at other collaborating institutes (FNAL, BINP, BNL, University of Manchester, The Cockcroft Institute, STFC) who supported the HEL study and made it possible to integrate HEL

2021 JINST 16 P03042

in the HL-LHC upgrade baseline. In particular, L. Rossi supported strongly, as HL-LHC project leader until 2020, this activity, and he is kindly acknowledged for that. B. Di Girolamo played a key role, as a link for in-kind collaborations, in the process to integrate the HEL in the HL-LHC. We would also like to acknowledge the various students and post-doc who worked on the subject during the past several years of studies (R. Cai, M. Fitterer, H. Garcia, G. Gobbi, V. Moens, V. Previtali, H. Rafique, S. Sadovich, J. Smith, J. Wagner), as well as G. Apollinari, V. Shiltsev and A. Valishev (FNAL); W. Fischer and X. Gu (BNL); G. Arduini, F. Bertinelli, R. Jones and H. Schmickler (CERN).

This manuscript has been authored by Fermi Research Alliance, LLC under Contract No. DE-AC02-07CH11359 with the U.S. Department of Energy, Office of Science, Office of High Energy Physics.

References

[1] O. Brüning, P. Collier, P. Lebrun, S. Myers, R. Ostojic, J. Poole et al., *LHC design report (Volume I, The LHC main ring)*, CERN Yellow Reports: Monographs, CERN, Geneva (2004) [DOI: 10.5170/CERN-2004-003-V-1].

[2] I. Béjar Alonso, O. Brüning, P. Fessia, L. Rossi, L. Tavian and M. Zerlauth, *High-Luminosity Large Hadron Collider (HL-LHC): Technical design report*, CERN Yellow Reports: Monographs, CERN, Geneva (2020), [DOI: 10.23731/CYRM-2020-0010].

[3] H. Damerau, A. Funken, R. Garoby, S. Gilardoni, B. Goddard, K. Hanke et al., *LHC Injectors Upgrade, Technical Design Report*, Tech. Rep., CERN-ACC-2014-0337 (2014).

[4] N. Fuster-Martínez et al., *Simulations of heavy-ion halo collimation at the CERN Large Hadron Collider: Benchmark with measurements and cleaning performance evaluation*, *Phys. Rev. Accel. Beams* **23** (2020) 111002 [arXiv:2008.03234].

[5] R. Assmann et al., *The final collimation system for the LHC*, *Conf. Proc. C* **060626** (2006) 986.

[6] R.W. Assmann, *Collimators and Beam Absorbers for Cleaning and Machine Protection*, in *Proceedings of the LHC Project Workshop — Chamonix XIV*, Chamonix, France, 17 January 2005, pp. 261–267.

[7] R. Bruce et al., *Simulations and measurements of beam loss patterns at the CERN Large Hadron Collider*, *Phys. Rev. ST Accel. Beams* **17** (2014) 081004 [arXiv:1409.3123].

[8] G. Valentino et al., *Final implementation, commissioning, and performance of embedded collimator beam position monitors in the Large Hadron Collider*, *Phys. Rev. Accel. Beams* **20** (2017) 081002.

[9] G. Valentino, R. Assmann, R. Bruce, S. Redaelli, A. Rossi, N. Sammut et al., *Semiautomatic beam-based LHC collimator alignment*, *Phys. Rev. ST Accel. Beams* **15** (2012) 051002.

[10] R. Bruce, R.W. Assmann and S. Redaelli, *Calculations of safe collimator settings and β^* at the CERN Large Hadron Collider*, *Phys. Rev. ST Accel. Beams* **18** (2015) 061001.

[11] R. Bruce, C. Bracco, R. De Maria, M. Giovannozzi, A. Mereghetti, D. Mirarchi et al., *Reaching record-low β^* at the CERN Large Hadron Collider using a novel scheme of collimator settings and optics*, *Nucl. Instrum. Meth. A* **848** (2017) 19.

[12] M. Lamont, *Status of the LHC*, *J. Phys. Conf. Ser.* **455** (2013) 012001.

[13] B. Salvachua et al., *Cleaning Performance of the LHC Collimation System up to 4 TeV*, in proceedings of the 4^{th} *International Particle Accelerator Conference*, Shanghai, China, 12–17 May 2013, MOPWO048.

[14] R. Bruce, N. Fuster-Martínez, A. Mereghetti, D. Mirarchi and S. Redaelli, *Review of LHC Run 2 Machine Configurations*, in proceedings of the 9^{th} *LHC Operations Evian Workshop*, Geneva, Switzerland, 30 January– 1 February 2019, pp. 187–197.

[15] S. Redaelli, R. Bruce, A. Lechner and A. Mereghetti, *Chapter 5: Collimation system*, in *High-Luminosity Large Hadron Collider (HL-LHC): Technical design report*, CERN Yellow Reports: Monographs, CERN, Geneva (2020), pp. 87–114.

[16] G. Valentino, R. Assmann, R. Bruce, F. Burkart, S. Redaelli, B. Salvachua et al., *Beam Diffusion Measurements Using Collimator Scans in the LHC*, *Phys. Rev. ST Accel. Beams* **16** (2013) 021003.

[17] A. Gorzawski, R.B. Appleby, M. Giovannozzi, A. Mereghetti, D. Mirarchi, S. Redaelli et al., *Probing LHC halo dynamics using collimator loss rates at 6.5 TeV*, *Phys. Rev. Accel. Beams* **23** (2020) 044802.

[18] V. Lebedev and V. Shiltsev, eds., *Accelerator Physics at the Tevatron Collider*, Springer-Verlag, New York (2014) [DOI: 10.1007/978-1-4939-0885-1].

[19] V. Shiltsev, *Tevatron: The world's first fully superconducting collider and the discovery of the top and bottom quarks*, in *Challenges and Goals for Accelerators in the XXI Century*, World Scientific (2016), pp. 211–222.

[20] *Review of the needs for a hollow e-lens for the HL-LHC*, CERN, Geneva, Switzerland, 6–7 October 2016 [https://indico.cern.ch/event/567839/].

[21] G. Arduini, R. Bruce, R. De Maria, M. Giovannozzi, G. Iadarola, J. Jowett et al., *Chapter 2: Machine layout and performance*, in *High-Luminosity Large Hadron Collider (HL-LHC): Technical design report*, CERN Yellow Reports: Monographs, CERN, Geneva (2020), pp. 17–46.

[22] D. Mirarchi, G. Arduini, M. Giovannozzi, A. Lechner, S. Redaelli and J. Wenninger, *Special Losses during LHC Run 2*, in 9^{th} *LHC Operations Evian Workshop*, Geneva, Switzerland, 30 January– 1 February 2019, pp. 213–220.

[23] R. Calaga, P. Baudrenghien, O. Capatina, E. Jensen and E. Montesinos, *Chapter 4: RF systems*, in *High-Luminosity Large Hadron Collider (HL-LHC): Technical design report*, CERN Yellow Reports: Monographs, CERN, Geneva (2020) pp. 65–86.

[24] A. Santamaria Garcia, *Experiment and Machine Protection from Fast Losses caused by Crab Cavities in the High Luminosity LHC*, PhD thesis, Ecole Polytechnique, Lausanne (2018) [DOI: 10.5075/epfl-thesis-8533].

[25] B. Lindström et al., *Fast failures in the LHC and the future high luminosity LHC*, *Phys. Rev. Accel. Beams* **23** (2020) 081001 [arXiv:2005.04520].

[26] A. Gorzawski, A. Abramov, R. Bruce, N. Fuster-Martínez, M. Krasny, J. Molson et al., *Collimation of partially stripped ions in the CERN Large Hadron Collider*, *Phys. Rev. Accel. Beams* **23** (2020) 101002 [arXiv:2007.12507].

[27] J. Coello de Portugal, R. Tomás, L. Fiscarelli, D. Gamba and M. Martino, *Impact of flux jumps in future colliders*, *Phys. Rev. Accel. Beams* **23** (2020) 011001.

[28] E. Metral, S. Antipov, F. Antoniou, R.B. Appleby, G. Arduini, J. Barranco Garcia et al., *Update of the HL-LHC operational scenarios for proton operation*, Tech. Rep., CERN-ACC-NOTE-2018-0002, (2018).

2021 JINST 16 P03042

[29] G. Stancari, A. Valishev, G. Annala, G. Kuznetsov, V. Shiltsev, D.A. Still et al., *Collimation with hollow electron beams*, *Phys. Rev. Lett.* **107** (2011) 084802 [arXiv:1105.3256].

[30] *U.S. LHC Accelerator Research Program*, https://www.uslarp.org.

[31] H. Pfeffer and G. Saewert, *A 6 kV Arbitrary Waveform Generator for the Tevatron Lens*, 2011 *JINST* **6** P11003 [arXiv:1209.4921].

[32] G. Stancari, *New Methods of Particle Collimation in Colliders*, in proceedings of *Meeting of the APS Division of Particles and Fields*, 2011 [arXiv:1110.0144].

[33] G. Stancari, G. Annala, T.R. Johnson, G.W. Saewert, V. Shiltsev, D.A. Still et al., *Collimation Studies with Hollow Electron Beams*, *Conf. Proc. C* **110904** (2011) 1939.

[34] G. Stancari, *Beam experience at the Tevatron and status of the hollow electron-lens hardware*, presented at the *Special Collimation Upgrade Specification Meeting: Internal Review of Tevatron Hollow Electron-Lens Usage at CERN*, CERN, Geneva, Switzerland, 9 November 2012, https://indico.cern.ch/event/213752.

[35] X. Gu et al., *Halo removal experiments with hollow electron lens in the BNL Relativistic Heavy Ion Collider*, *Phys. Rev. Accel. Beams* **23** (2020) 031001.

[36] X. Gu et al., *The electron lens test bench for the relativistic heavy ion collider at Brookhaven National Laboratory*, *Nucl. Instrum. Meth. A* **743** (2014) 56.

[37] D. Pierini et al., *Design of high-performance guns for the HL-LHC HEL*, in *ICFA Beam Dynamics Newsletter #81* (2021).

[38] S. Li and G. Stancari, *Characterization of an Electron Gun for Hollow Electron Beam Collimation*, Tech. Rep., FERMILAB-TM-2542-APC, Fermilab (2012).

[39] D. Nikiforov, M. Arsentyeva, A. Levichev, A. Barnyakov and A. Rossi, *Electron dynamics for high-intensity hollow electron beams*, in *ICFA Beam Dynamics Newsletter #81* (2021).

[40] D. Mirarchi et al., *Nonlinear dynamics of proton beams with hollow electron lens in the CERN High-Luminosity LHC*, submitted to *Eur. Phys. J. Plus* (2021).

[41] A. Goldblatt, E. Bravin, T. Mitsuhashi, F. Roncarolo and G. Trad, *Design and Performance of Coronagraph for Beam Halo Measurements in the LHC*, in proceedings of *International Beam Instrumentation Conference*, Barcelona, Spain, 11–15 Sep 2016, pp. 253–256.

[42] F. Schmidt, *SIXTRACK version 1.2: single particle tracking code treating transverse motion with synchrotron oscillations in a symplectic manner; user's reference manual*, Tech. Rep., CERN-SL-94-56-AP, CERN, Geneva (1994).

[43] http://sixtrack.web.cern.ch/SixTrack/.

[44] G. Robert-Demolaize, R. Assmann, S. Redaelli and F. Schmidt, *A new version of SixTrack with collimation and aperture interface*, in proceedings of the*Particle Accelerator Conference*, Knoxville, TN, U.S.A., 16–20 May 2005, pp. 4084–4086.

[45] http://lhc-collimation-project.web.cern.ch/lhc-collimation-project/code-tracking-2012.php.

[46] CERN, *ICFA Mini-Workshop on Tracking for Collimation in Particle Accelerators*, CERN, Geneva, Switzerland, 30 October 2015 [DOI: 10.23732/CYRCP-2018-002].

[47] P.D. Hermes, R. Bruce, J.M. Jowett, S. Redaelli, B. Salvachua Ferrando, G. Valentino et al., *Measured and simulated heavy-ion beam loss patterns at the CERN Large Hadron Collider*, *Nucl. Instrum. Meth. A* **819** (2016) 73.

2021 JINST 16 P03042

[48] R. Bruce et al., *Collimation-induced experimental background studies at the CERN Large Hadron Collider*, *Phys. Rev. Accel. Beams* **22** (2019) 021004.

[49] A. Gorzawski, A. Abramov, R. Bruce, N. Fuster-Martínez, M. Krasny, J. Molson et al., *Collimation of partially stripped ions in the CERN Large Hadron Collider*, *Phys. Rev. Accel. Beams* **23** (2020) 101002 [arXiv:2007.12507].

[50] D. Mirarchi et al., *Reducing Beam-Related Background on Forward Physics Detectors Using Crystal Collimation at the Large Hadron Collider*, *Phys. Rev. Applied* **14** (2020) 064066.

[51] M. Fitterer, G. Stancari, a. Valishev, R. De Maria, S. Redaelli, K. Sjobak et al., *Implementation of Hollow Electron Lenses in SixTrack and First Simulation Results for the HL-LHC*, in proceedings of the *8th International Particle Accelerator Conference*, Copenhagen, Denmark, 14–19 May 2017, THPAB041.

[52] R. Bruce et al., *Status of SixTrack with collimation*, in proceedings of *ICFA Mini-Workshop on Tracking for Collimation in Particle Accelerators*, CERN Yellow Reports: Conference Proceedings, vol. 2, 2018, pp. 1–10.

[53] V. Previtali, G. Stancari, A. Valishev and S. Redaelli, *Numerical Simulations of a Hollow Electron Lens as a Scraping Device for the LHC*, in proceedings of the *4th International Particle Accelerator Conference*, Shanghai, China, 12–17 May 2013, MOPWO044.

[54] V. Previtali, G. Stancari, A. Valishev and S. Redaelli, *Numerical simulations of a proposed hollow electron beam collimator for the LHC upgrade at CERN*, Tech. Rep., FERMILAB-TM-2560-APC, Fermilab (2013).

[55] M. Fitterer, G. Stancari, A. Valishev, S. Redaelli and D. Valuch, *Resonant and random excitations on the proton beam in the Large Hadron Collider for active halo control with pulsed hollow electron lenses*, *Phys. Rev. Accel. Beams* **24** (2021) 021001 [arXiv:1804.07418].

[56] A. Mereghetti, *Status of simulations and required inputs*, presented at the *122nd Collimation Upgrade Specification Meeting*, November 2019, https://indico.cern.ch/event/865924/ [DOI: 10.5281/zenodo.4623944].

[57] W. Hofle et al., *LHC Transverse Feedback System and its Hardware Commissioning*, in probeedings of the *11th European Particle Accelerator Conference*, Genoa, Italy, 23–27 June 2008, THPC121.

2021 JINST 16 P03042